Ab initio lattice stability in comparison with CALPHAD lattice stability

Y. Wang[a], S. Curtarolo[b], C. Jiang[a], R. Arroyave[a], T. Wang[a], G. Ceder[c], L.-Q. Chen[a], Z.-K. Liu[a],*

[a]*Materials Science and Engineering, Pennsylvania State University, State College, PA 16802, United States*
[b]*Department of Mechanical Engineering and Materials Science, Duke University, Durham, NC 27708, United States*
[c]*Department of Materials Science and Engineering, MIT, Cambridge, MA 02139, United States*

Abstract

A systematic first-principles calculation for the total energies of 78 pure elemental solids has been performed at zero Kelvin using the projector augmented-wave method within the generalized gradient approximation. The total energy differences, i.e. lattice stabilities, among the face-centered-cubic (fcc), body-centered-cubic (bcc), and hexagonal-close-packed (hcp) crystal structures are studied and compared with the Scientific Group Thermodata Europe (SGTE) database developed by the CALPHAD method. For non-transitional elements, favorable comparison is observed, while for the majority of transition elements, particularly the V, Cr, Mn, Fe, and Co group elements, significant discrepancies exist. The Bain/tetragonal distortion analysis between fcc and bcc structures shows that when one structure is stable, the other is unstable, and the higher the energy of the unstable structure, the larger the discrepancy. Through analysis of the alloying effect in binary systems, we conclude that the lattice stability of unstable structures obtained through extrapolation of first-principles calculations in binary systems is close to the SGTE lattice stability obtained by the CALPHAD method.
© 2004 Elsevier Ltd. All rights reserved.

1. Introduction

Over the past decades, CALPHAD (CALculation of PHAse Diagram) thermodynamic modeling has been widely recognized as a powerful tool in predicting multi-component phase diagrams and guiding new materials development. CALPHAD modeling begins with the evaluation of descriptions of pure elements and binary systems. By combining the constitutive binary systems and ternary experimental data, ternary interactions and Gibbs energy of ternary phases are obtained. Thermodynamic databases thus developed cover the whole composition and temperature ranges, including experimentally uninvestigated regions. In this approach, the modeling of Gibbs energies of individual phases and the coupling of phase diagram and thermochemistry are the key components in developing internally consistent thermodynamic descriptions of multicomponent materials with sound fundamentals and predictive power. It is self-evident that the relative Gibbs energies of a pure element in various competing crystal structures, i.e., the so-called lattice stability, are the foundation of the CALPHAD approach [1,2]. The primary methods used to derive the lattice stability data for pure elements include direct measurements, extrapolations from activity measurements, and critical assessment of data for a large number of binary systems.

During the last decade, the first-principles methodology for calculating total energies of solids has become increasingly sophisticated. Using only the atomic number and atom positions as input [3], the total energy of a crystal structure can be accurately calculated, and the relative lattice stability between two different crystal structures and the formation energy of a compound can be evaluated at 0 K. Skriver [4] carried out systematic calculations for pure elements with the linear muffin-tin orbital (LMTO) method within the atomic-sphere approximation (ASA) and local density approximation (LDA).

* Corresponding author. Tel.: +1 814 865 1934; fax: +1 412 291 3185.
E-mail address: liu@matse.psu.edu (Z.-K. Liu).

The thermodynamic data for 78 pure elements used by SGTE (Scientific Group Thermodata Europe) were published for various phase structures [5,6]. This data set has been widely adopted within the international community as a basis for thermodynamic modeling of multicomponent systems. However, it was found that agreement between the SGTE data and the first-principles results was rather poor for most of the transition metals [2] and this has been an outstanding issue in computational thermodynamics [7–9].

The primary reason for the discrepancy seems due to the structural instability of transition metals [8,9] in some crystal structures, with possible minor contributions from the limitation of earlier first-principles approach and the fact that first-principles data were obtained at 0 K while the SGTE data is evaluated for 298 K.

In this work, we systematically calculated the relative lattice stabilities among face-centered-cubic (fcc), body-centered-cubic (bcc), and hexagonal-close-packed (hcp) structures across the periodic table using the ab initio density functional pseudopotential method. Furthermore, we performed first-principles calculations in selected binary systems with fcc, bcc, or hcp structures to understand the discrepancies between the first-principles data and the SGTE data.

2. Ab initio approach

For pure elements, energy calculations were carried out using density functional theory [3], in the generalized gradient approximation (GGA), with projector augmented-wave (PAW) pseudo-potentials, as implemented in VASP [10–12]. For the GGA correlation energy, we used the Perdew–Wang parameterization (GGA-PW91) [13]. Calculations are at 0 K without pressure and zero-point motion. The PAW method is the state of the art in electronic calculations because it is almost as fast as the usual ultrasoft pseudopotential (US-PP) method [12,14], and gives energies very close to the best full-potential linearized augmented-plane-wave (FLAPW) calculations [10,11,15]. The energy cut-off was set to 1.75 times the suggested energy cut-off for the corresponding element pseudopotential, derived by the method described in [12].

Brillouin zone integrations were performed using 4000/(number of atoms in unit cell) k-points distributed as uniformly as possible on a Monkhorst–Pack mesh. We verified that with these energy cut-offs and k-point meshes, the absolute energy is converged to better than 10 meV/atom for sample calculations. Energy differences between structures are expected to be converged to much smaller tolerances. Spin polarization was used in all calculations, and all structures were fully relaxed.

We selected the 78 most important elements from the periodic table. The total energies were calculated for bcc, fcc, and hcp structures. It should be mentioned that certain structures do not exist naturally, for example, the Cr-fcc. Due to the large number of calculations required, we adopted the "High Throughput ab initio computing" scheme, described in [16,17].

For binary systems, our main focus is on the calculations of the effect of Bain/tetragonal distortions on the stability of the system. To save computer time, such calculations were carried out using Vanderbilt ultrasoft pseudopotentials (US-PP) within GGA. For pure Mo, the transformation energy from bcc to fcc is very similar in US-PP (39.66 kJ/mol) and PAW (38.74 kJ/mol). Three compositions were typically selected, i.e. 25%, 50%, and 75%, and energies of formation were calculated by systematically varying the c/a ratio of a unit cell along the Bain/tetragonal distortion path. Four binary systems were selected to explore the effects of structure and alloy composition on structure instability, i.e. Al–Cu, Al–Ni, Mo–Ni, and Mo–Ta.

3. Results and discussions

In this section, we present our results for pure elements and compare with the SGTE data [6], the suggested data by Saunders et al. [5], and the previous first-principles calculations [4]. Combined with the results from binary systems, we attempt to shed some light on the discrepancies in the lattice stability between the first-principles and SGTE data.

3.1. Total energy for the bcc, fcc, and hcp structures

The calculated total energies for the 78 selected elements in the fcc, bcc, and hcp structures are listed in Tables 1, 2 and 3, respectively. Although these total energies are referred to the infinite separation of the pseudo-atoms, they do not represent the cohesive energies of the solids since the referenced electronic states used in the atomic pseudopotentials are not the ground states of the atoms. These total energies are usually not available in the literature, but are critically important in calculating lattice stabilities of different crystal structures. The stable structures of each element at room temperature are also included in Table 1 for convenience. For the elements whose ground states were bcc, fcc, or hcp, a comparison between the calculated and the experimental lattice parameters [18] was carried out. It was found that the calculated lattice parameters agreed very well with experimentally determined ones, with the difference being less than 2.5% for the great majority of the elements. An exception to this was observed for Cd, Eu, and Tl, where the differences between experiments and calculations were between 2.5% and 3.2%. This disagreement could be attributed to deficiencies in the pseudopotentials used.

3.2. Energy difference—lattice stability

In this section, our discussions are focused on the lattice stability between bcc and fcc ($E_i^{bcc-fcc} = E_i^{bcc} - E_i^{fcc}$) (Table 4) and between hcp and fcc ($E_i^{hcp-fcc} = E_i^{hcp} - E_i^{fcc}$) (Table 5). The SGTE data [6] and the data suggested by

Table 1
The calculated bcc lattice constant and total energy using VASP with PAW-GGA potential

Li	Be											B	C	N	O	F
3.442	2.505											2.313	2.381			
−1.8976	−3.6046											−4.9213	−4.8349	–	–	–
bcc	hcp											rhomb	diamond			
Na	**Mg**											**Al**	**Si**	**P**	**S**	**Cl**
4.197	3.571		←	bcc lattice constant in Å	→							3.244	3.112	3.076	3.168	
−1.3165	−1.4528		←	total energy in eV/atom	→							−3.6012	−4.8468	−4.6498	−3.0245	
bcc	hcp		←	room temperature structure	→							fcc	diamond	complex	complex	
K	**Ca**	**Sc**	**Ti**	**V**	**Cr**	**Mn**	**Fe**	**Co**	**Ni**	**Cu**	**Zn**	**Ga**	**Ge**	**As**	**Se**	**Br**
5.271	4.362	3.666	3.241	2.992	2.847	2.792	2.822	2.809	2.799	2.886	3.137	3.378	3.389	3.368	3.443	3.758
−1.0384	−1.8997	−6.1185	−7.7002	−8.9632	−9.4655	−8.8117	−8.2748	−6.8834	−5.2954	−3.6082	−1.0269	−2.8504	−4.1302	−4.2373	−2.9450	−1.0369
bcc	fcc	hcp	hcp	bcc	bcc	complex	bcc	hcp	fcc	fcc	hcp	complex	diamond	rhomb	hex	–
Rb	**Sr**	**Y**	**Zr**	**Nb**	**Mo**	**Tc**	**Ru**	**Rh**	**Pd**	**Ag**	**Cd**	**In**	**Sn**	**Sb**	**Te**	**I**
5.661	4.736	4.029	3.574	3.322	3.178	3.094	3.068	3.082	3.145	3.306	3.623	3.814	3.840	3.789	3.852	4.149
−0.9292	−1.6197	−6.2577	−8.3598	−10.0466	−10.7799	−9.9384	−8.4677	−6.8033	−5.1001	−2.7032	−0.7060	−2.5503	−3.7409	−3.9182	−2.8581	−1.0833
bcc	fcc	hcp	hcp	bcc	bcc	hcp	hcp	fcc	fcc	fcc	hcp	tetr	diamond	rhomb	hex	complex
Cs	**Ba**		**Hf**	**Ta**	**W**	**Re**	**Os**	**Ir**	**Pt**	**Au**	**Hg**	**Tl**	**Pb**	**Bi**	**Po**	**At**
6.122	5.006		3.538	3.320	3.190	3.125	3.099	3.120	3.175	3.319	3.883	3.970	4.009	4.005		
−0.8573	−1.9233		−9.6562	−11.7358	−12.7781	−11.9107	−10.2440	−8.1765	−5.9637	−3.1829	−0.1957	−2.2301	−3.5042	−3.7182		
bcc	bcc		hcp	bcc	bcc	hcp	hcp	fcc	fcc	fcc	–	hcp	fcc	rhomb	Sc	–
		La	**Ce**	**Pr**	**Nd**	**Pm**	**Sm**	**Eu**	**Gd**	**Tb**	**Dy**	**Ho**	**Er**	**Tm**	**Yb**	**Lu**
		4.219	3.772	4.161	4.122	4.096	4.066	4.429	4.027	4.006	3.987	3.969	3.947	3.933		3.896
		−4.7823	−5.7318	−4.6262	−4.5791	−4.5436	−4.4984	−1.8587	−4.4549	−4.4213	−4.3882	−4.3574	−4.3384	−4.3158		−4.2813
		hex	fcc	hex	hex	–	complex	bcc	hcp	hcp	hcp	hcp	hcp	hcp	fcc	hcp
Fr	**Ra**	**Ac**	**Th**	**Pa**	**U**	**Np**	**Pu**	**Am**	**Cm**	**Bk**	**Cf**	**Es**	**Fm**	**Md**	**No**	**Lr**
		4.494	4.018	3.677	3.437	3.294	3.207									
–	–	−3.9339	−7.2039	−9.2207	−10.8731	−12.3007	−13.4703		–	–	–	–	–	–	–	–
		fcc	fcc	tetr	complex	complex	complex	hex								

Table 2
The calculated fcc lattice constant and total energy using VASP with PAW-GGA potential

Li	Be											B	C	N	O	F
4.321	3.150											2.873	3.096			
−1.9002	−3.6273											−5.2818	−4.6306			
Na	**Mg**											**Al**	**Si**	**P**	**S**	**Cl**
5.305	4.516				fcc lattice constant in Å →							4.048	3.936	3.897	4.002	
−1.3175	−1.4670				total energy in eV/atom →							−3.6967	−4.8272	−4.4836	−2.8416	
K	**Ca**	**Sc**	**Ti**	**V**	**Cr**	**Mn**	**Fe**	**Co**	**Ni**	**Cu**	**Zn**	**Ga**	**Ge**	**As**	**Se**	**Br**
6.634	5.501	4.600	4.099	3.810	3.619	3.502	3.446	3.518	3.517	3.631	3.939	4.234	4.284	4.268	4.343	4.707
−1.0392	−1.9165	−6.1786	−7.7498	−8.7150	−9.0845	−8.8885	−8.1872	−6.9696	−5.3902	−3.6379	−1.0885	−2.8657	−4.1376	−4.1263	−2.7929	−1.0074
Rb	**Sr**	**Y**	**Zr**	**Nb**	**Mo**	**Tc**	**Ru**	**Rh**	**Pd**	**Ag**	**Cd**	**In**	**Sn**	**Sb**	**Te**	**I**
7.143	6.000	5.046	4.529	4.230	4.014	3.886	3.827	3.847	3.972	4.155	4.500	4.792	4.855	4.792	4.842	5.195
−0.9299	−1.6242	−6.3615	−8.3972	−9.7232	−10.3784	−10.1357	−8.9748	−7.1390	−5.1389	−2.7267	−0.7570	−2.5609	−3.7512	−3.8253	−2.7421	−1.0702
Cs	**Ba**		**Hf**	**Ta**	**W**	**Re**	**Os**	**Ir**	**Pt**	**Au**	**Hg**	**Tl**	**Pb**	**Bi**	**Po**	**At**
7.756	6.313		4.471	4.224	4.043	3.928	3.866	3.880	3.985	4.173	4.926	4.988	5.049	5.057		
−0.8585	−1.9065		−9.7613	−11.4896	−12.3115	−12.1685	−10.9790	−8.7920	−6.0451	−3.2026	−0.1808	−2.2155	−3.5478	−3.6695		
		La	**Ce**	**Pr**	**Nd**	**Pm**	**Sm**	**Eu**	**Gd**	**Tb**	**Dy**	**Ho**	**Er**	**Tm**	**Yb**	**Lu**
		5.260	4.710	5.242	5.208	5.154	5.121	5.628	5.046	5.022	4.994	4.967	4.942	4.917		4.873
		−4.9090	−5.9640	−4.7458	−4.7035	−4.6735	−4.6320	−1.8420	−4.5905	−4.5557	−4.5201	−4.4855	−4.4613	−4.4328		−4.3839
Fr	**Ra**	**Ac**	**Th**	**Pa**	**U**	**Np**	**Pu**	**Am**	**Cm**	**Bk**	**Cf**	**Es**	**Fm**	**Md**	**No**	**Lr**
		5.649	5.048	4.668	4.439	4.353	4.760									
		−4.0641	−7.3485	−9.3978	−10.7657	−12.0606	−13.5919									

Table 3
The calculated hcp lattice constant and total energy using VASP with PAW-GGA potential

Legend: hcp lattice constant a in Å; c/a; total energy in eV/atom

Li	Be											B	C	N	O	F
3.064	2.259											2.876	2.154			
1.639	1.583											0.6196	1.636			
−1.9007	−3.7093											−6.0978	−4.6947			

Na	Mg											Al	Si	P	S	Cl
3.745	3.189											2.870	2.676	2.765	3.365	
1.634	1.621											1.640	1.760	1.617	1.045	
−1.3175	−1.4796											−3.6672	−4.8610	−4.5227	−3.2938	

K	Ca	Sc	Ti	V	Cr	Mn	Fe	Co	Ni	Cu	Zn	Ga	Ge	As	Se	Br
4.635	3.892	3.310	2.929	2.605	2.485	2.485	2.456	2.494	2.483	2.558	2.660	3.003	3.022	2.960	3.666	3.349
1.619	1.650	1.555	1.580	1.799	1.786	1.618	1.583	1.614	1.647	1.652	1.856	1.633	1.632	1.742	1.049	1.632
−1.0365	−1.9135	−6.2250	−7.8069	−8.7095	−9.0751	−8.9197	−8.2676	−6.9902	−5.3681	−3.6325	−1.1183	−2.8586	−4.1404	−4.1764	−3.1648	−0.9763

Rb	Sr	Y	Zr	Nb	Mo	Tc	Ru	Rh	Pd	Ag	Cd	In	Sn	Sb	Te	I
5.062	4.249	3.654	3.230	2.880	2.767	2.764	2.732	2.741	2.785	2.928	3.061	3.391	3.400	3.350	4.088	3.336
1.629	1.643	1.546	1.606	1.821	1.768	1.598	1.582	1.612	1.671	1.655	1.833	1.631	1.634	1.703	1.067	1.952
−0.9301	−1.6203	−6.3836	−8.4354	−9.7551	−10.3666	−10.2034	−9.0866	−7.1052	−5.1130	−2.7237	−0.7674	−2.5573	−3.7564	−3.8661	−2.9830	−1.0599

Cs	Ba		Hf	Ta	W	Re	Os	Ir	Pt	Au	Hg	Tl	Pb	Bi	Po	At
5.493	4.450		3.200	2.898	2.781	2.785	2.759	2.753	2.769	2.927	3.517	3.569	3.559	3.537		
1.626	1.640		1.580	1.780	1.783	1.615	1.581	1.622	1.734	1.675	1.610	1.587	1.642	1.653		
−0.8592	−1.9106		−9.8320	−11.4579	−12.2928	−12.2334	−11.1164	−8.7241	−5.9931	−3.2018	−0.2007	−2.2343	−3.5291	−3.7130		

		La	Ce	Pr	Nd	Pm	Sm	Eu	Gd	Tb	Dy	Ho	Er	Tm	Yb	Lu
		3.753	3.288	3.717	3.684	3.674	3.652	3.944	3.626	3.614	3.604	3.592	3.576	3.552		3.511
		1.627	1.746	1.629	1.617	1.606	1.597	1.656	1.578	1.570	1.561	1.553	1.550	1.558		1.558
		−4.8817	−5.8759	−4.7244	−4.6834	−4.6552	−4.6161	−1.8395	−4.5828	−4.5532	−4.5244	−4.4977	−4.4817	−4.4606		−4.4239

Fr	Ra	Ac	Th	Pa	U	Np	Pu	Am	Cm	Bk	Cf	Es	Fm	Md	No	Lr
		4.007	3.552	3.190	2.986	2.799	3.454									
		1.627	1.680	1.782	1.835	2.165	1.510									
		−4.0558	−7.3070	−9.3927	−10.9294	−12.2058	−13.5847									

Table 4
Lattice stability $E^{\mathrm{bcc-fcc}}$ (kJ/mol)

Li	**Be**											**B**	**C**	**N**	**O**	**F**
0.25	2.19											34.73	−19.71			
0.11	0.04															
0.11	0.50												−6.00			
Na	**Mg**											**Al**	**Si**	**P**	**S**	**Cl**
0.10	1.37				←—— VASP-PAW-GGA ——→							9.21	−1.89	−16.04	−17.65	
0.05	0.50				←—— SGTE data ——→							10.08	−4.00	7.95		
0.05	0.50				←—— Saunders et al. ——→							10.08	−4.00			
K	**Ca**	**Sc**	**Ti**	**V**	**Cr**	**Mn**	**Fe**	**Co**	**Ni**	**Cu**	**Zn**	**Ga**	**Ge**	**As**	**Se**	**Br**
0.08	1.62	5.80	4.79	−23.95	−36.76	7.41	−8.45	8.31	9.15	2.87	5.94	1.48	0.71	−10.71	−14.68	−2.85
−0.05	1.41	−3.02	0.48	−7.50	−6.13	0.78	−7.97	1.71	7.99	4.02	−0.08	0.70	−1.90			
−0.05	0.93			−15.30	−9.19	1.80		4.20	7.49	4.02	6.03	0.70	−1.90			
Rb	**Sr**	**Y**	**Zr**	**Nb**	**Mo**	**Tc**	**Ru**	**Rh**	**Pd**	**Ag**	**Cd**	**In**	**Sn**	**Sb**	**Te**	**I**
0.07	0.43	10.02	3.61	−31.20	−38.74	19.04	48.93	32.39	3.74	2.27	4.92	1.02	0.99	−8.96	−11.19	−1.26
−0.20	1.33	1.19	−0.29	−13.50	−15.20	8.00	9.00	19.00	10.50	3.40		0.64	−1.11			
−0.20	0.75			−22.00	−28.00	8.00	14.00	19.00	10.50	3.40		0.65	0.25			
Cs	**Ba**		**Hf**	**Ta**	**W**	**Re**	**Os**	**Ir**	**Pt**	**Au**	**Hg**	**Tl**	**Pb**	**Bi**	**Po**	**At**
0.12	−1.62		10.14	−23.75	−45.02	24.87	70.92	59.39	7.85	1.90	−1.43	−1.41	4.20	−4.70		
−0.50	−1.80		2.38	−16.00	−19.30	6.00	14.50	32.00	15.00	4.25		−0.09	2.40	1.40		
−0.50	−1.80		−4.14	−26.50	−33.00	18.20	30.50	32.00	15.00	4.25		0.07	2.40			

La	**Ce**	**Pr**	**Nd**	**Pm**	**Sm**	**Eu**	**Gd**	**Tb**	**Dy**	**Ho**	**Er**	**Tm**	**Yb**	**Lu**
12.22	22.40	11.56	12.00	12.53	12.89	−1.61	13.08	12.97	12.73	12.36	11.86	11.29		9.90

Fr	**Ra**	**Ac**	**Th**	**Pa**	**U**	**Np**	**Pu**	**Am**	**Cm**	**Bk**	**Cf**	**Es**	**Fm**	**Md**	**No**	**Lr**
		12.56	13.95	17.09	−10.36	−23.17	11.73									

Table 5
Lattice stability $E^{\text{hcp–fcc}}$ (kJ/mol)

Values are listed in order: VASP-PAW-GGA, SGTE data, Saunders et al.

Element	VASP-PAW-GGA	SGTE data	Saunders et al.
Li	−0.05	−0.05	−0.05
Be	−7.91	−6.35	−6.35
B	−67.84		
C	−6.18		−3.00
N			
O			
F			
Na	0.03	−0.05	−0.05
Mg	−1.22	−2.60	−2.60
Al	2.85	5.48	5.48
Si	−3.26	−1.80	−1.80
P	−3.77		
S	−43.63		
Cl			
K	0.26		0.00
Ca	0.29	0.50	0.50
Sc	−4.48	−5.00	
Ti	−5.51	−6.00	−6.00
V	0.53	−3.50	−4.80
Cr	0.91	−2.85	−1.82
Mn	−3.01	−1.00	−1.00
Fe	−7.76	−2.24	
Co	−1.99	−0.43	−0.43
Ni	2.13	2.89	1.50
Cu	0.52	0.60	0.60
Zn	−2.88	−2.97	
Ga	0.69	0.70	0.70
Ge	−0.27	−1.00	−1.00
As	−4.83		
Se	−35.88		
Br	3.00		
Rb	−0.02		0.00
Sr	0.38	0.25	0.25
Y	−2.13	−6.00	
Zr	−3.69	−7.60	−7.60
Nb	−3.08	−3.50	−5.00
Mo	1.14	−3.65	−5.00
Tc	−6.53	−10.00	−10.00
Ru	−10.79	−12.50	−12.50
Rh	3.26	3.00	3.00
Pd	2.50	2.00	2.00
Ag	0.29	0.30	0.30
Cd	−1.00	−0.89	
In	0.35	0.37	0.65
Sn	−0.50	−1.61	−0.25
Sb	−3.94		
Te	−23.24		
I	0.99		
Cs	−0.07		0.00
Ba	−0.40	0.20	0.20
Hf	−6.82	−10.00	−10.00
Ta	3.06	−4.00	−6.50
W	−1.78	−4.55	−6.00
Re	−6.26	−11.00	−11.00
Os	−13.26	−13.00	−13.00
Ir	6.55	4.00	4.00
Pt	5.02	2.50	2.50
Au	0.08	0.24	0.55
Hg	−1.92	−2.07	
Tl	−1.81	−0.31	−0.31
Pb	1.80	0.30	0.30
Bi	−4.20		
Po			
At			

La	Ce	Pr	Nd	Pm	Sm	Eu	Gd	Tb	Dy	Ho	Er	Tm	Yb	Lu
2.63	8.50	2.08	1.94	1.77	1.53	0.24	0.74	0.24	−0.41	−1.18	−1.97	−2.68		−3.86

Fr	Ra	Ac	Th	Pa	U	Np	Pu	Am	Cm	Bk	Cf	Es	Fm	Md	No	Lr
		0.80	4.00	0.49	−15.79	−14.01	0.69									
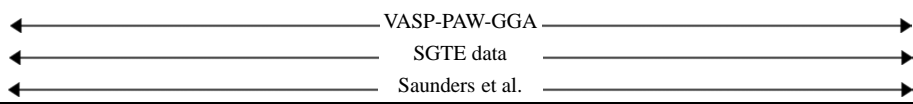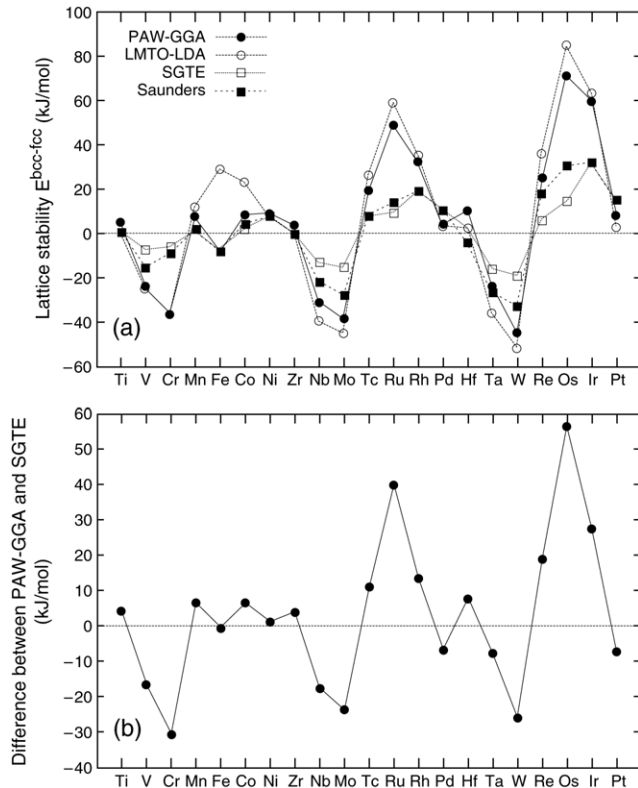
Fig. 1. (a) Lattice stability between bcc and fcc, $E^{bcc-fcc}$, for selected elements. ●: This work (calculation using GGA); ○: Skriver ([4], calculation using LDA); □: SGTE data [6]; ■: Saunders [5]. (b) Difference between PAW-GGA and SGTE.

Fig. 2. (a) Lattice stability between hcp and fcc, $E^{hcp-fcc}$, for selected elements. ●: This work (calculation using GGA); ○: Skriver ([4], calculation using LDA); □: SGTE data [6]; ■: Saunders et al. [5]. (b) Difference between PAW-GGA and SGTE.

Saunders et al. [5] are included in the tables for comparison. It is noted in Table 4 that the relative stability between fcc and bcc for Bi (A7), Cs (A2), Ge (A4), K (A2), Rb (A2), Sc (A3), Sn (A5), Zn (A3), and Zr (A3) (the designation in parenthesis represents the stable structure at room temperature in the terminology of *Strukturbericht* symbols [19]) is different between the current PAW-GGA calculations and the SGTE data. The same is true between fcc and hcp for Ba, Cr, Li, Mo, Na, Ta, and V as shown in Table 5, which all have bcc as the stable structure at room temperature. These differences are relatively small in most cases, and further detailed investigations are needed to understand them completely, taking into account the entropy contributions.

From Tables 4 and 5, one can see that for non-transition metal elements, the differences between the SGTE data and our PAW-GGA data are typically around 1–2 kJ/mol or less, while for some transition metal elements, the differences can be quite large, for example, as high as about 54 kJ/mol for $E_{Os}^{bcc-fcc}$ and about 40 kJ/mol for $E_{Ru}^{bcc-fcc}$. Figs. 1(a) and 2(a) plot the lattice stability between bcc and fcc, $E_i^{bcc-fcc}$, and between hcp and fcc, $E_i^{hcp-fcc}$, together with previous first-principles calculated data [4], those by Saunders et al. [5], and the SGTE data [6]. Figs. 1(b) and 2(b) present the differences between present PAW-GGA data and the SGTE data, for elements from the Ti group to the Ni group,

respectively. One can see that the agreement between the present data and the SGTE data is better than those between previous first-principles calculated data [4] and the SGTE data, particularly for $E_{Fe}^{bcc-fcc}$ which have different signs. It is also noted that the discrepancies between present PAW-GGA and SGTE data are larger between fcc and bcc than those between fcc and hcp when judged by absolute values.

The discrepancies between the SGTE data and the first-principles results, particularly for fcc–bcc lattice stability, pose a dilemma. On one hand, the SGTE data have been tested on many systems with great success. On the other hand, the first-principles method has been demonstrated to be successful in many fields, especially for the close-packed structures. In the following, we discuss the discrepancies in terms of the stabilities of pure elements, effect of alloying elements, and the accessibility by experiments.

3.3. Elastic/mechanical instability along tetragonal transformation

The large differences between the first-principles calculations and the SGTE data could partly be attributed to the instability [8] of the higher-energy phases, the entropies of which at finite T become abnormal [20]. Grimvall [8] discussed the discrepancies between CALPHAD and ab initio calculations in terms of the instability of the fcc
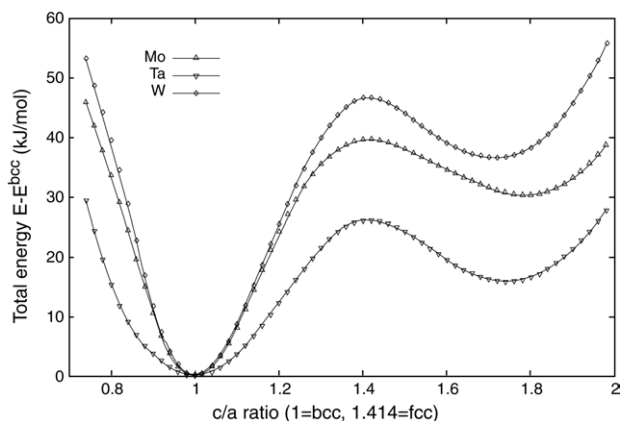
Fig. 3. Total energy, $E - E^{bcc}$, along the tetragonal transformation path for Mo, Ta, and W.

Fig. 4. Total energy, $E - E^{fcc}$, along the tetragonal transformation path for Ni, Al, and Cu.

Fig. 5. Total energy, $E - E^{hcp}$, along the tetragonal transformation path for Ru and Os.

structure for bcc transition metals and argued that "obviously one should not take H (enthalpy) from ab initio calculations, unless one has the reasons to believe that the description chosen for S (entropy) is adequate".

The lattice instabilities along the Bain/tetragonal transformation path of the cubic metals had been studied by many authors [9,21–25] as it represents the transformation between fcc and bcc structures. This instability is demonstrated for bcc Mo, Ta, W in Fig. 3 and for fcc Al, Cu, Ni in Fig. 4. It is shown that the fcc structure of bcc Mo, Ta, and W is a local maximum with respect to the Bain deformation, and the higher the maximum is, the larger the discrepancy between the SGTE data and the present PAW-GGA data, while for fcc Al, Cu, Ni, the bcc structure is at a local maximum. Our results are similar to those by Wang et al. [9] who studied the total energy profiles along the tetragonal, trigonal, and hexagonal transformation paths with volumes fixed at experimental values using the FLAPW-LDA method implemented in the WIEN97 package [26]. Using the assumed tetragonal lattice, we also studied the lattice instabilities along the Bain/tetragonal transformation path for the hcp metals Ru and Os as shown in Fig. 5. The behavior of energy against c/a ratio of these two hcp metals is very similar to those of fcc metals.

We can conclude that an fcc structure for elements with bcc being the ground state or a bcc structure for elements with fcc being the ground state, is unstable with respect to the Bain distortion. The same is true between bcc and hcp through the hexagonal transformation as demonstrated by Wang et al. [9]. There have been no exceptions for all elements that have been calculated so far.

For an unstable structure, the harmonic description of its vibrational entropy is thermodynamically incorrect since the potential surface seen by the lattice ion can no longer be approximated by a parabola [8,20,27]. If an unstable structure of a pure element is stabilized at high temperatures, its entropy has to be abnormal. In many cases, unstable structures never become stable. Their enthalpy and entropy are thus not physically defined at all. Therefore, if their
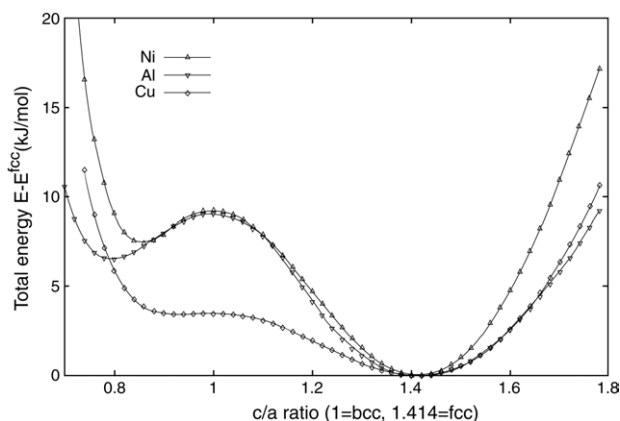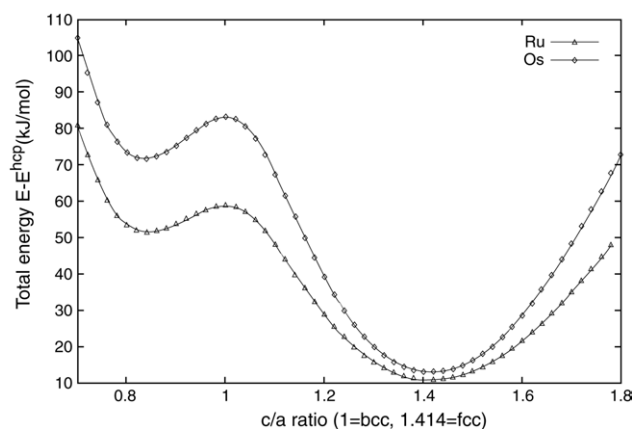
mathematical values are needed for the purpose of modeling, one would need to extrapolate from stable region to unstable (or experimentally inaccessible) region for both enthalpy and entropy. Whether the extrapolation is arbitrary depends on how far apart the two regions are and how many binary systems are used for the extrapolation.

It is thus evident that all calculated lattice stability between fcc and bcc would endure this intrinsic instability no matter how large the discrepancy is between the first-principles calculations and the SGTE data. Consequently, by examining the stability or the phonon spectrum of pure elements alone, one cannot predict how large the discrepancy would be between the first-principles calculations and the SGTE data. Instead, one should investigate the effects of various alloying elements because they stabilize unstable structures.

3.4. Effect of alloying elements

It is mentioned above that the major reason for the large deviations between the first-principles and SGTE lattice stability should be related to mechanical instabilities. The addition of a second element must produce a large energy of
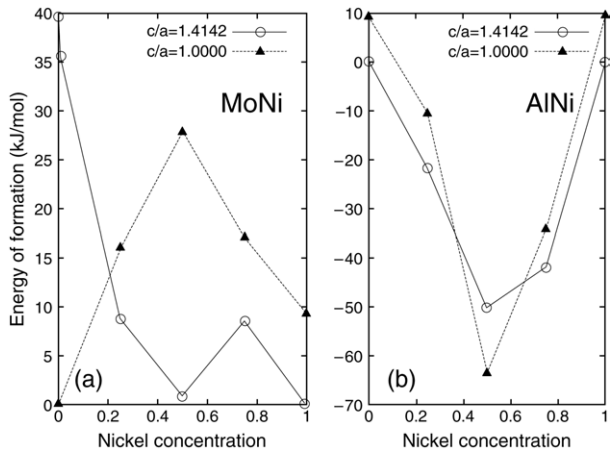
Fig. 6. Energies of formation of fcc- and bcc-based structures: (a) Mo–Ni; (b) Al–Ni.

Fig. 7. Energy along the tetragonal transformation path for Mo, Mo_3Ni, MoNi, $MoNi_3$, and Ni with respect to E_{bcc}^{Mo} and E_{fcc}^{Ni}.

Fig. 8. Energy along the tetragonal transformation path for Al, Al_3Ni, AlNi, $AlNi_3$, and Ni with respect to E_{Al}^{fcc} and E_{Ni}^{fcc}.

formation (negative) to make an unstable structure at least metastable if it is to be experimentally accessible. We first tested this in the Ni–Mo system.

Keeping the atoms in the parent fcc sites with volume relaxation only, we calculated the energies of formation for the ordered compounds, $NiMo_{107}$, $NiMo_3$, $NiMo$, Ni_3Mo, and $Ni_{107}Mo$. The results are plotted in Fig. 6(a). On the Mo-rich side, it is noted that the addition of Ni makes the energy of formation decrease rapidly as a function of Ni concentration. As mentioned before, the SGTE database was developed by means of the CALPHAD method where extrapolation from different compositions is used whenever an element is not stable in a particular lattice type (as is the case for fcc Mo). If one made a linear extrapolation using first-principles data of $NiMo_3$ and NiMo, the estimated energy of formation of pure fcc Mo would be about 16 kJ/mol, much closer to the SGTE data of about 15.20 kJ/mol than the direct first-principles result of about 40 kJ/mol. Thus, this extrapolation methodology could provide a numerical approximation for the lattice stability of unstable structures, which can in turn be used in CALPHAD thermodynamic assessments. It is worth noting that this extrapolation is essentially equivalent to the CALPHAD method, with the data points obtained through ab initio calculations, instead of experiments. The results with the parent bcc structure in Mo–Ni are also shown in Fig. 6(a). We can see that with one Ni atom added to 107 Mo atoms in fcc, the energy has dropped more than 10% in comparison with pure Mo, and the linear interpolation gives the bcc and fcc stability cross-over composition around 20% Mo. A comparable study for the Ni–Al system was also performed and the results are shown in Fig. 6(b).

Using the tetragonal structure, we have also calculated the energy curves as functions of both c/a ratio and composition for the representative Mo–Ni, Al–Ni, Al–Cu, and Mo–Ta binary systems. We have studied the effect of composition by considering the tetragonal transformations of the B2 structure and $L1_2$ structures at three different compositions:
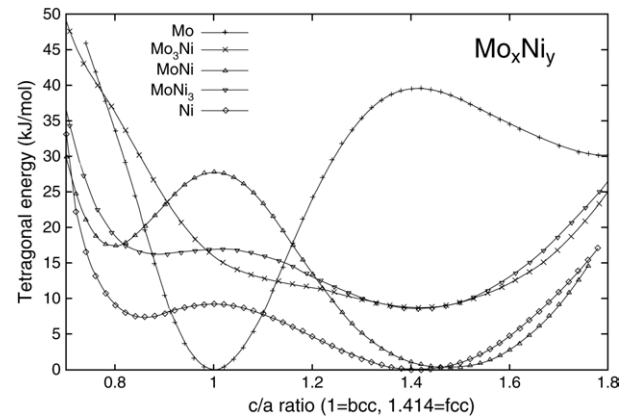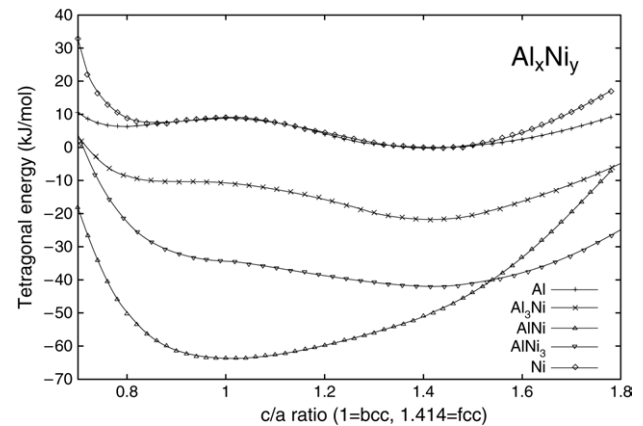
25%, 50%, and 75%. The results are plotted in Figs. 7–10. The following observations can be made for these systems:

3.4.1. Mo–Ni (Fig. 7)

Since the ground states of Mo and Ni are bcc and fcc, respectively, the stability of the bcc and fcc structures will switch when the composition changes from pure Mo to pure Ni as shown in Fig. 6. Fig. 7 further shows that 25% Ni in Mo has made the fcc-based structure stable along the tetragonal transformation path, and the bcc-based structure is unstable at 25% Ni with respect to the tetragonal transformation. The energy of formation is decreased to about 10 kJ/mol for 25% Ni from the value of 40 kJ/mol for fcc Mo.

3.4.2. Al–Ni (Fig. 8)

The ground states of both Al and Ni are fcc. It is surprising to observe that the bcc (B2) structure is stable along the tetragonal transformation at the 50% Ni concentration. In addition, this agrees with the experimental Al–Ni phase diagram, in which a large B2 phase region is
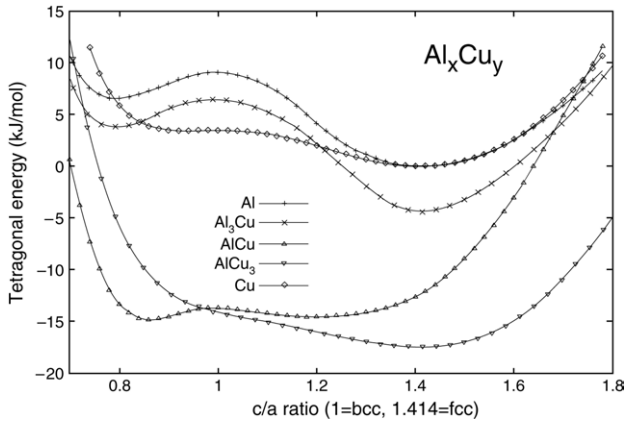
Fig. 9. Energy along the tetragonal transformation path for Al, Al_3Cu, AlCu, $AlCu_3$, and Cu with respect to E_{Al}^{fcc} and E_{Cu}^{fcc}.
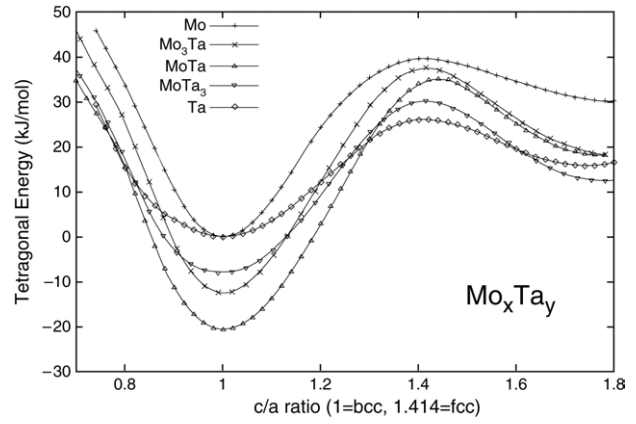
Fig. 10. Energy along the tetragonal transformation path for Mo, Mo_3Ta, MoTa, $MoTa_3$, and Ta with respect to E_{Mo}^{bcc} and E_{Ta}^{bcc}.

observed and the B2 phase is stable in the whole temperature range from room temperature to melting [28].

3.4.3. Al–Cu (Fig. 9)

Both Al and Cu have the fcc ground state. The energy curve for the 50% Cu concentration has the shape of a double well, and neither fcc ($L1_0$) nor bcc (B2) is at the energy minimum along the tetragonal transformation. Rather the bcc (B2) structure is at an energy maximum and unstable with respect to the tetragonal transformation. The almost equal depths of the two energy wells and small energy barrier between wells might be related to the stability of the bcc phase and contribute to the complex phase relations at high temperatures in Al–Cu [29]. At other Cu compositions, the fcc-based structure is the most stable one, similar to Al–Ni.

3.4.4. Mo–Ta (Fig. 10)

Both Mo and Ta have the bcc ground state. To date, no experimental evidence shows that they can transform into any other solid structures at temperature up to melting points and at pressure up to 300 GPa (see [30,31] and references therein). The energy curves for all the concentrations show that only the bcc-based structures are stable.

The above observations indicate that the ground states of pure elements largely determine the stability along the tetragonal transformation path, but for composition ranges near 50%, non-ground-state structures may become stable.

3.5. Significance of experimental accessibility

In this section, we focus on metallic elements, for which systematic differences between the present calculations and the SGTE data [6] can be observed. The largest difference occurs between bcc and fcc energies (see Fig. 1) for the V, Cr, Mn, Fe, and Co groups with Cr, Mo, Os, Ru, and W showing maximum values (over 30 kJ/mol), for which no direct experimental data are available in the fcc structure. For the Ti group where both the bcc and hcp structures can exist
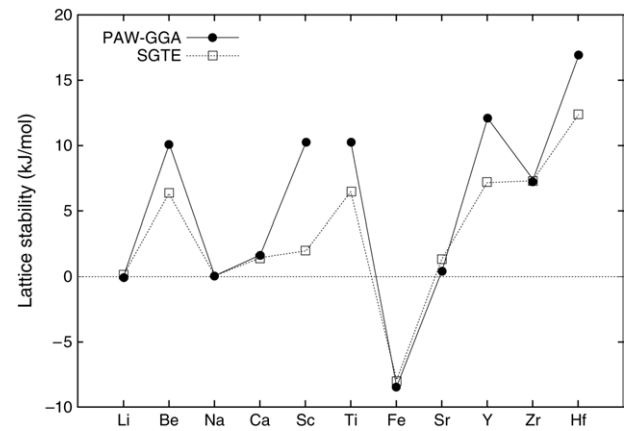
Fig. 11. Comparisons of lattice stability between the present GGA values and the SGTE data: $E_{Li}^{bcc-hcp}$, $E_{Be}^{bcc-hcp}$, $E_{Na}^{bcc-hcp}$, $E_{Ca}^{bcc-fcc}$, $E_{Sc}^{bcc-hcp}$, $E_{Ti}^{bcc-hcp}$, $E_{Fe}^{bcc-fcc}$, $E_{Sr}^{bcc-fcc}$, $E_{Y}^{bcc-hcp}$, $E_{Zr}^{bcc-hcp}$, and $E_{Hf}^{bcc-hcp}$; for them both the bcc and the closed-packed (fcc or hcp) structure are accessible experimentally. ●: This work (calculation using GGA); □: SGTE data [6].

naturally at high temperatures, the present calculations agree well with the SGTE data. For Fe, the experimental data are available for both bcc and fcc, and the agreement is within 1 kJ/mol.

Our PAW-GGA lattice stabilities between bcc and fcc or hcp for elements with both structures accessible experimentally under atmospheric pressures are shown in Fig. 11 in comparison with the SGTE data [6]. In contrast to the lattice stability of Cr, Mo, Os, Ru, and W, these elements show considerably smaller discrepancy between the present PAW-GGA and SGTE data. This is understandable because the energy difference between bcc and fcc or hcp would be lower if both structures were experimentally accessible at different temperatures.

4. Summary

We have calculated the relative enthalpies among the bcc, fcc, and hcp structures using the first-principles approach

across the periodic table. The results are compared with the data used in the SGTE database [6], the suggested data by Saunders et al. [5] and previous first-principles calculations [4]. It is realized that the discrepancy between first-principles and SGTE data is intrinsic because when the element has either fcc or bcc as its ground state, it is unstable in bcc or fcc, respectively, with respect to tetragonal distortion. For an unstable structure, frequencies for some of the phonon modes would become imaginary, and the first-principles results cannot be interpreted directly. On the other hand, the unstable structures could be stabilized in binary solutions through alloying with other elements having this structure as its ground state. The CALPHAD lattice stability of an unstable structure can thus be obtained by extrapolations based on first-principles calculations of energies of formation, at different compositions, in binary systems with respect to the stable structures of the two elements.

Acknowledgements

References

[1] L. Kaufman, H. Bernstein, Computer Calculation of Phase Diagram, Academic Press Inc., New York, 1970.

[2] N. Saunders, A.P. Miodownik, CALPHAD (Calculation of Phase Diagrams): A Comprehensive Guide, Pergamon, Oxford, New York, 1998.

[3] W. Kohn, L. Sham, Physical Review 140 (1965) 1133–1138.

[4] H.L. Skriver, Physical Review B 31 (1985) 1909–1923.

[5] N. Saunders, A.P. Miodownik, A.T. Dinsdale, Calphad-Computer Coupling of Phase Diagrams and Thermochemistry 12 (1988) 351–374.

[6] A.T. Dinsdale, CALPHAD 15 (1991) 317–425.

[7] J. Houserova, J. Vřeštál, M. Friak, M. Sob, Calphad-Computer Coupling of Phase Diagrams and Thermochemistry 26 (2002) 513–522.

[8] G. Grimvall, Berichte Der Bunsen-Gesellschaft-Physical Chemistry Chemical Physics 102 (1998) 1083–1087.

[9] L.G. Wang, M. Sob, Z.Y. Zhang, Journal of Physics and Chemistry of Solids 64 (2003) 863–872.

[10] G. Kresse, D. Joubert, Physical Review B 59 (1999) 1758–1775.

[11] P.E. Blochl, Physical Review B 50 (1994) 17953–17979.

[12] G. Kresse, Vienna ab initio simulation package (VASP), http://cms.mpi.univie.ac.at/vasp/vasp/vasp.html, 2003.

[13] J.P. Perdew, Y. Wang, Physical Review B 45 (1992) 13244–13249.

[14] D. Vanderbilt, Physical Review B 41 (1990) 7892–7895.

[15] P.A. Serena, A. Baratoff, J.M. Soler, Physical Review B 48 (1993) 2046–2056.

[16] S. Curtarolo, D. Morgan, K. Persson, J. Rodgers, G. Ceder, Physical Review Letters 91 (2003) 135503.

[17] S. Curtarolo, D. Morgan, G. Ceder, High-throughput ab initio computing: transition metal binary alloys, 2004 (submitted for publication).

[18] WebElements, http://www.webelements.com/, 2004.

[19] Crystal Lattice-Structures, http://cst-www.nrl.navy.mil/lattice/, 2004.

[20] Y. Wang, R. Ahuja, M.C. Qian, B. Johansson, Journal of Physics—Condensed Matter 14 (2002) L695–L701.

[21] P.J. Craievich, M. Weinert, J.M. Sanchez, R.E. Watson, Physical Review Letters 72 (1994) 3076–3079.

[22] P.J. Craievich, J.M. Sanchez, Computational Materials Science 8 (1997) 92–99.

[23] L.G. Wang, M. Sob, Physical Review B 60 (1999) 844–850.

[24] F. Jona, P.M. Marcus, Physical Review B 6309 (2001).

[25] P.M. Marcus, F. Jona, S.L. Qiu, Physical Review B 66 (2002).

[26] P. Blaha, K. Schwarz, G. Madsen, D. Kvasnicka, J. Luitz, WIEN2K, http://www.wien2k.at/, 2004.

[27] A.F. Guillermet, V. Ozolins, G. Grimvall, M. Korling, Physical Review B 51 (1995) 10364–10374.

[28] W. Huang, Y.A. Chang, Intermetallics 7 (1999) 625–626.

[29] J.L. Murray, in: D.E. Laughlin (Ed.), Phase Diagrams of Binary Copper Alloys, ASM International, Materials Park, OH, 1994, pp. 18–40.

[30] H. Cynn, C.S. Yoo, Physical Review B 59 (1999) 8526–8529.

[31] Y.K. Vohra, A.L. Ruoff, Physical Review B 42 (1990) 8651–8654.